



Reservoir Description, Diagenesis and Reservoir Quality of the Deep Marine Sediments in the Propagation Stage of Rift Basin

Kassem AA*

Exploration Department, Gulf of Suez Petroleum Company (GUPCO), Egypt

*Corresponding author: Ahmed A Kassem, Exploration Department, Gulf of Suez Petroleum Company (GUPCO), Egypt, Tel: +201229808046; Email: kassemaa@gmail.com

Research Article

Volume 6 Issue 4

Received Date: October 27, 2022

Published Date: November 22, 2022

DOI: 10.23880/ppej-16000316

Abstract

The exploration and exploitation of the downthrown side of the productive upthrown Pre-rifting reservoirs at the Gulf of Suez marked bring a renaissance to the rift basin Exploration. This work documents the reservoir performance, trap geometry, and structural style of the downthrown deep marine stratigraphic entrapment. In addition, it outlines the requirements necessary beyond the production mitigations and limits. To gain better understanding of Asl Formation (deep marine) reservoir characteristics early in the exploration program, Asl Formation was cored in the north October J-5 well. A continuous 366-foot (112m) core was recovered including the main reservoir interval, which is producing over 12,000 barrel of oil per day. The J-5 Asl Formation has been interpreted as a synthetic, mixed clastic-carbonate turbidity deposit. Three major lithofacies described are recognizable on electric log. These are sandstone, shale and carbonates. The sandstones dominate the lower portion of the core and are the main oil producing section. Sandstone porosity and permeability range from 17 to 27% and 30 millidarcies to 3 darcies, respectively. Compared to the sandstone, the carbonate turbidites have poorer reservoir quality. They dominate the upper portion of the core and are composed of coarse fossil debris, silica framework grains and rock fragments. Horizontal and vertical permeabilities with rock types. Both the sandstone and carbonate sections of the J-5 core have experienced a complex diagenetic history. Deposition of the cored interval was initiated by a convulsive geological event such as flashflood or earthquake. These events would likely generate sufficient energy for mobilization of onshore and/or near shore sediments into multiple gravity flows having regional extent. The reservoir quality is controlled by a combination of primary depositional fabric and subsequent diagenetic modification. This research work can guide future exploration of reservoir-prone deep marine deposits in the Red Sea Rift and provide a reference for the subsurface deep-water reservoir quality analysis in the propagation stage in the Rift Basins.

Keywords: Rift basins; Facies analysis; Diagenesis; Reservoir quality; Deep marine; Clastic reservoirs; Gulf of Suez

Introduction

The purpose of this paper is to provide a description and depositional environment interpretation of the Asl

Formation from a 366 ft (112m) conventional core taken in the J-5 well in the Gulf of Suez rift basin. North October Field is located in the northern portion of the Gulf of Suez basin, northwest of the main October Field (Figure 1). The

Asl Formation is stratigraphically located within the Upper Rudeis portion of the Miocene Tertiary section (Figure 2). It lies within the synrift sequence of the Gulf of Suez rift basin. The Asl is one of four producing reservoirs in the October Field [1]. The other three reservoirs are the Nukhul Formation (Lower Miocene), the Nezzazat Group (Cretaceous) and the Nubia Succession (Cretaceous to Carboniferous) (Figure 2). The Asl Formation produces from the downthrown side of the major October boundary fault which approximately 5000 ft (1524m) of displacement in north October area. Both the Nezzazat and Nubia succession produce from structurally high pre-Miocene tilted fault blocks [2]. The Nukhul Formation in North October, in contrast, produces from Stratigraphic punch-out at the Pre-Miocene level across the eastern edge of the high blocks [3]. This study focuses on the J-5 well drilled from the J-platform (Figure 1). The Gulf of Suez Basin rifting started in the Oligocene-Miocene period, and is considered an iconic rift basin that hosts excellent hydrocarbon reserves in the pre-rift and syn-rift sediments [2,4-7]. The structural and resulting stratigraphic complexity arises from the origin of the Gulf of Suez as a rift system [3,8]. The Gulf of Suez is known as the Clysmic Gulf, as presented by Robson [4] as a NW-SE trending depression. Therefore, the term "Clysmic" refers to the Gulf of Suez trend. The Early Miocene Upper Rudeis Formation consisted of Asl and Hawara members. It is widespread deep marine sediment in the Gulf of Suez. The underlying Hawara Member shale is a LST deposit too, with age and facies equivalent to the deep distal Asl Member system [9-11]. During the Early Miocene, initial isostatic uplift (Clysmic phase) and rotation of the rift shoulders rearranged the drainage systems that delivered sediment into the basin [9].

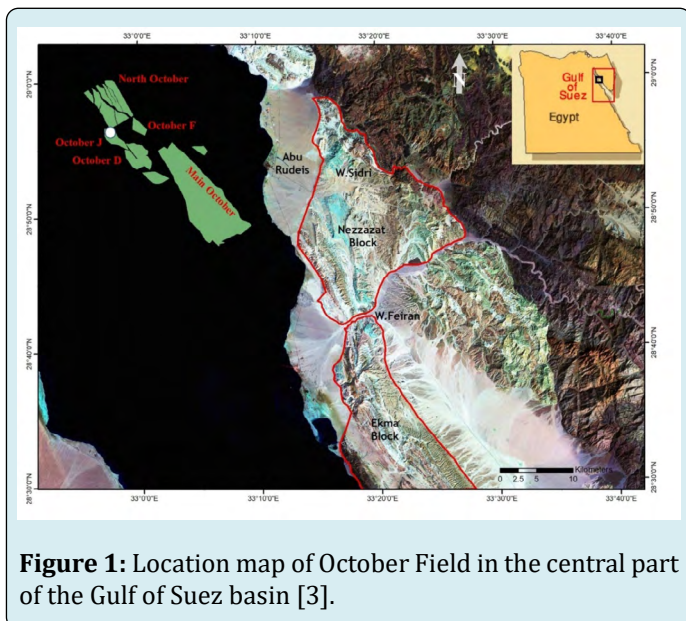


Figure 1: Location map of October Field in the central part of the Gulf of Suez basin [3].

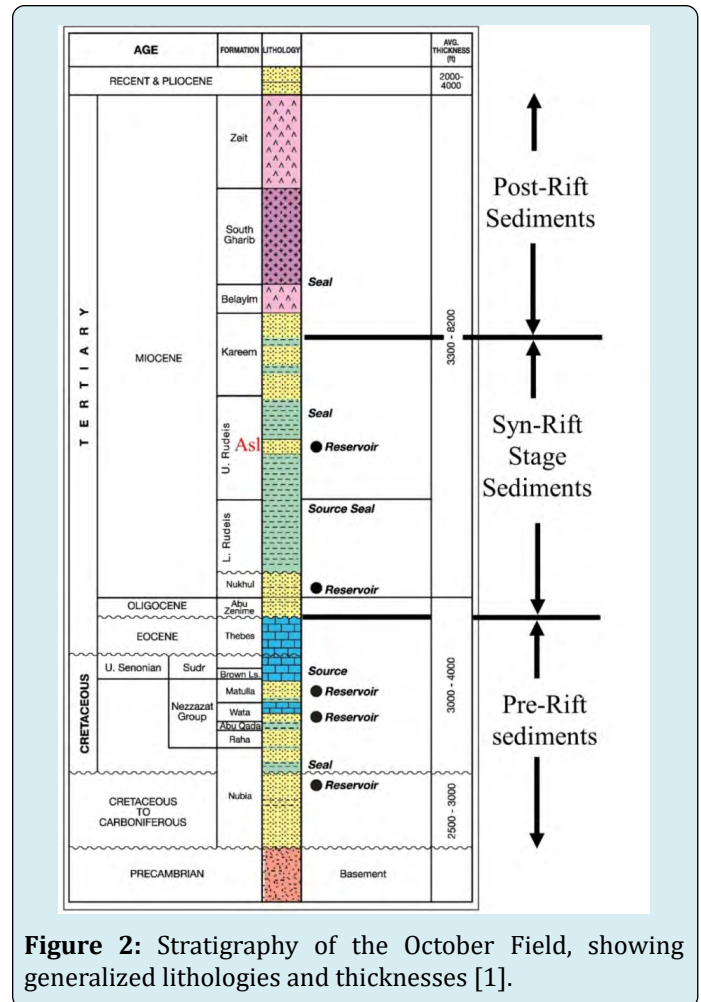


Figure 2: Stratigraphy of the October Field, showing generalized lithologies and thicknesses [1].

This paper aims to: (a) classify the sedimentological and petrological characteristics of the sediments formed during the propagation phase of rifting; (b) determine the depositional framework and diagenetic overprint that control the reservoir quality, and (d) investigate the geologic controls on reservoir properties, porosity/permeability relationships, and internal heterogeneities within clastic and carbonate lithofacies.

Results and Discussion

Lithofacies Description and Interpretations

The basal portion of the Asl Member in the well OCT-J5 core contains the best reservoir quality sandstones, which diminish upward into interbedded coarse-grained sandy carbonates of poor reservoir quality (Figures 3 & 4). The main sandstone interval at the base is about 200 ft thick; two thin net sand zones occur at shallower intervals within the core. From the core description (Figure 4), three main lithofacies have been interpreted as (A) sandstones, including imbricated clasts, broken laminations, and dewatering

features; (B) 2 ft-thick shale units; and (C) carbonates. Within the lithofacies, there are 14 reactivation surfaces. These are surfaces marked by a change in texture and/or composition along with bedding that represents boundaries between fining upward major depositional episodes (Figure 4). Interpreted lithofacies boundaries always correspond to reactivation surfaces, but reactivation surfaces may not always correspond to lithofacies boundaries (Figure 4).

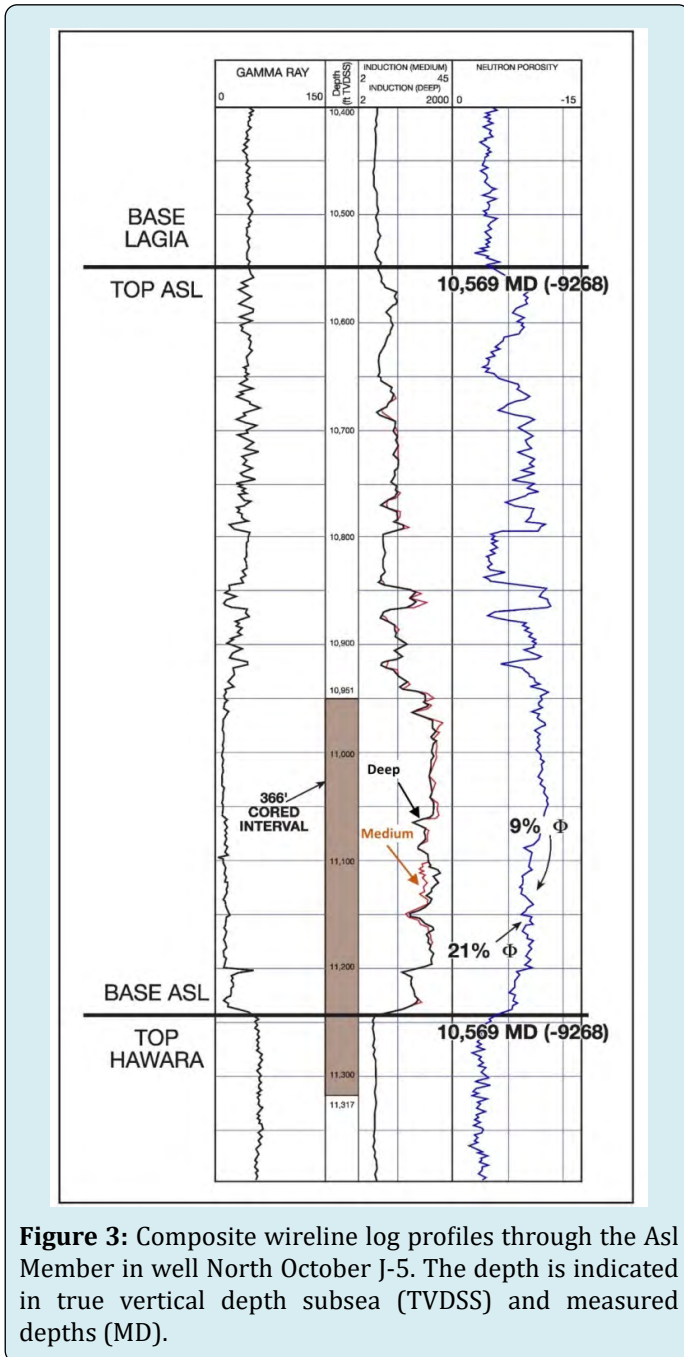
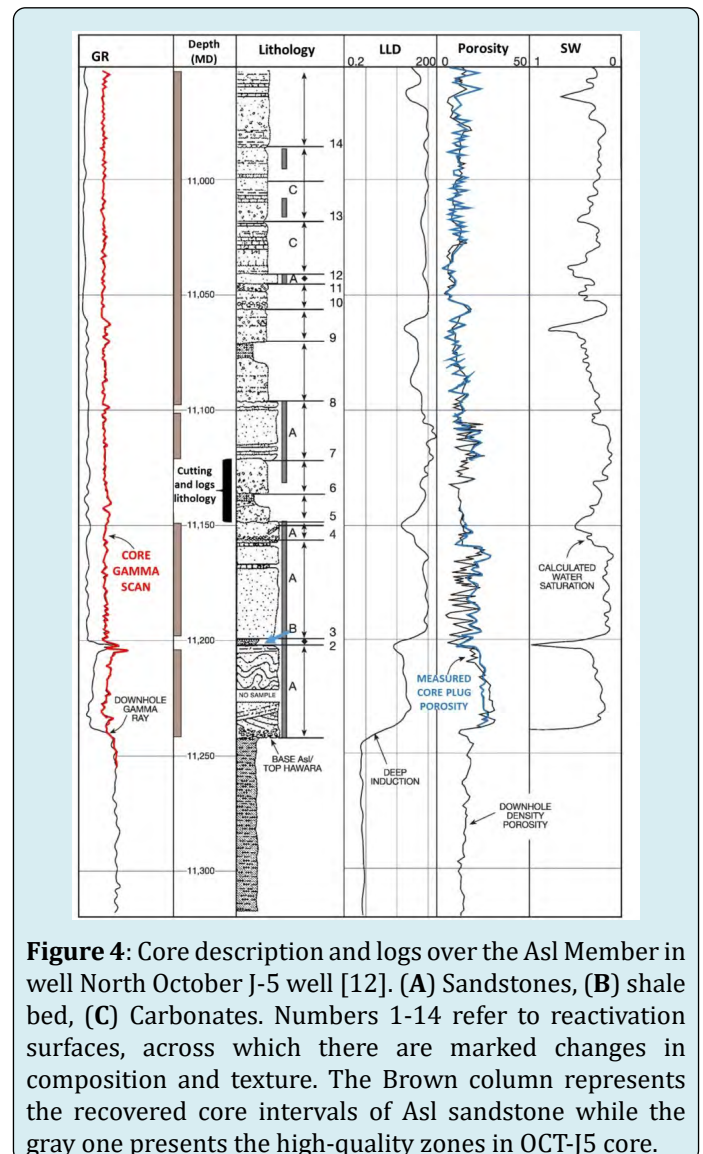
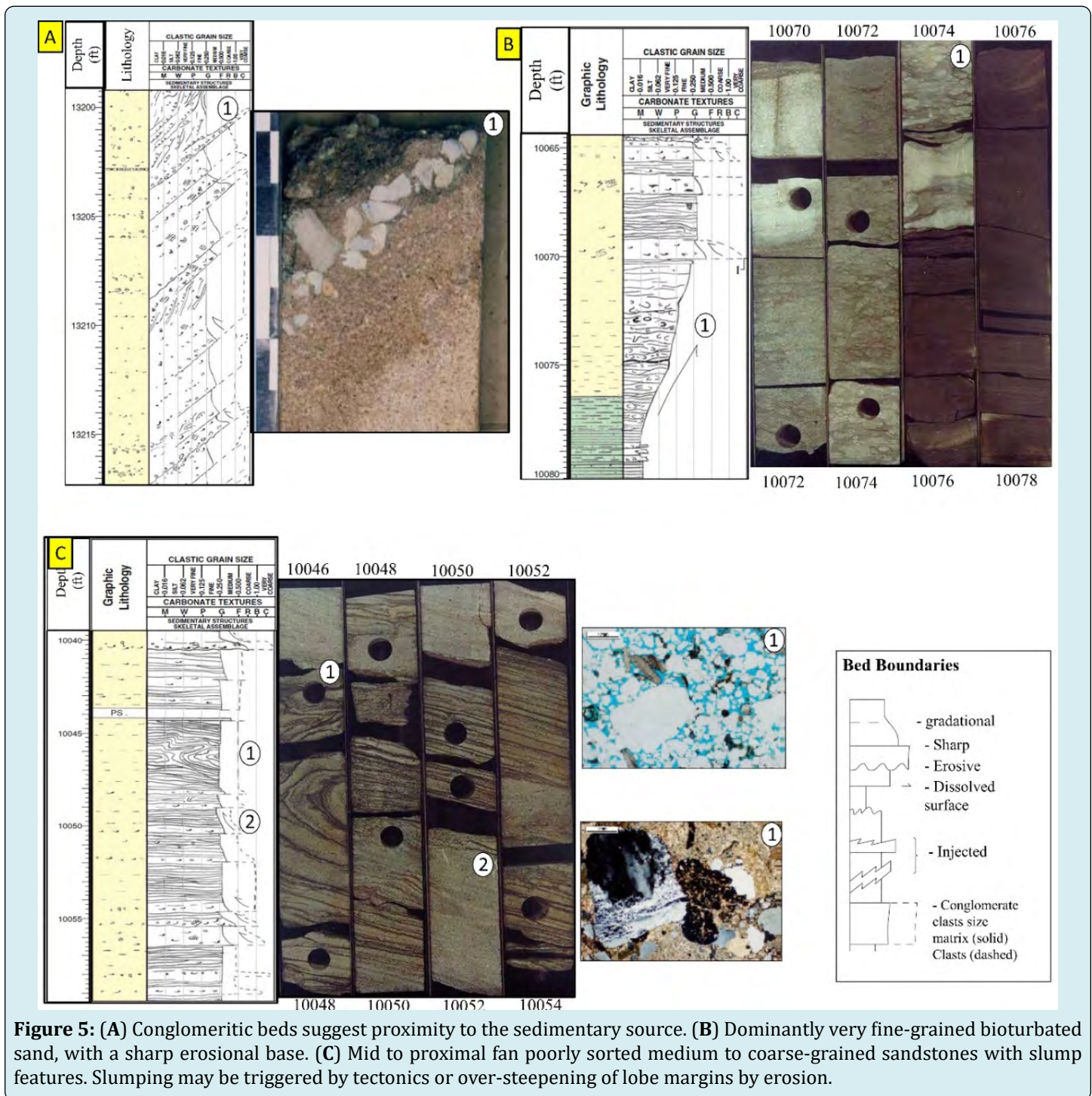


(Figure 4). A 366 ft core from well OCT-J5 has an upward fining sequence in the lower Asl sandstone (Figure 4) [12]. At the base, 200 ft of sandstones with the best reservoir quality pass upward into interbedded coarse-grained sandy carbonates with two thin sandstone beds (gray columns in Figure 4). The sandstone and carbonate lithofacies boundaries show strong oil staining in the sandstone, and weak stain in the overlying white to tan carbonates (Figure 5). This is due to the lower permeability in the carbonate lithofacies, which hold a higher volume of irreducible oil. Regionally, the underlying Hawara shale lithofacies is a pelagic deep-water shale deposits. In the OCT-J5 core, it is a uniform deposit, dark brown to black, and fissile. This lithofacies is bioturbated in the upper 5 ft of the core showing both vertical and horizontal burrows (Figure 5B), indicating a subaqueous depositional environment. The contact between Asl and Hawara rock units is marked by the deposition of sandstone rip-up clasts.



Therefore, the lithofacies boundaries can be tracked laterally in the un-cored intervals by their surface responses



Seventy thin sections through the cored interval were examined petrographically to help determine the texture and composition of the lithofacies as shown below.

Sandstone lithofacies (A): Sandstone lithofacies-A with the highest oil flow rates and staining (Figure 6), was deposited at the lower part of the Asl Member (Figure 3). It made up

of very fine-to-coarse sand sized and angular to subrounded grains, moderately to very well sorted. monocrystalline quartz grains are more common than feldspar grains (5-27%, average 9%) (Figure 7A). Fossil fragments, sedimentary rock fragments, pelletal glauconite, and metamorphic rock fragments are less abundant grains (Figure 7B-F). The binding material include kaolinite (less than 5%)

matrix (Figure 7B) calcite and dolomite cement (up to 20%) commonly developed and partially filling the leached skeletal grains (Figure 7E). The skeletal fragments; including mollusca, bryozoa, foraminifera, and corals (Figure 7D-F) some of the skeletal grains had been altered into glauconite pellets (Figure 7C). This sandstone are characterized by the presence of clean intergranular pores (Figure 7). Meanwhile,

intragranular pores (Figure 7) formed by the effect of dissolution of feldspars (Figure 7A) and moldic formed by dissolution of fossil fragments (Figure 7D-E). Quartz overgrowth is slightly common (Figures 7B, E, and F). The compositional percent quoted above was estimated visually from thin sections.

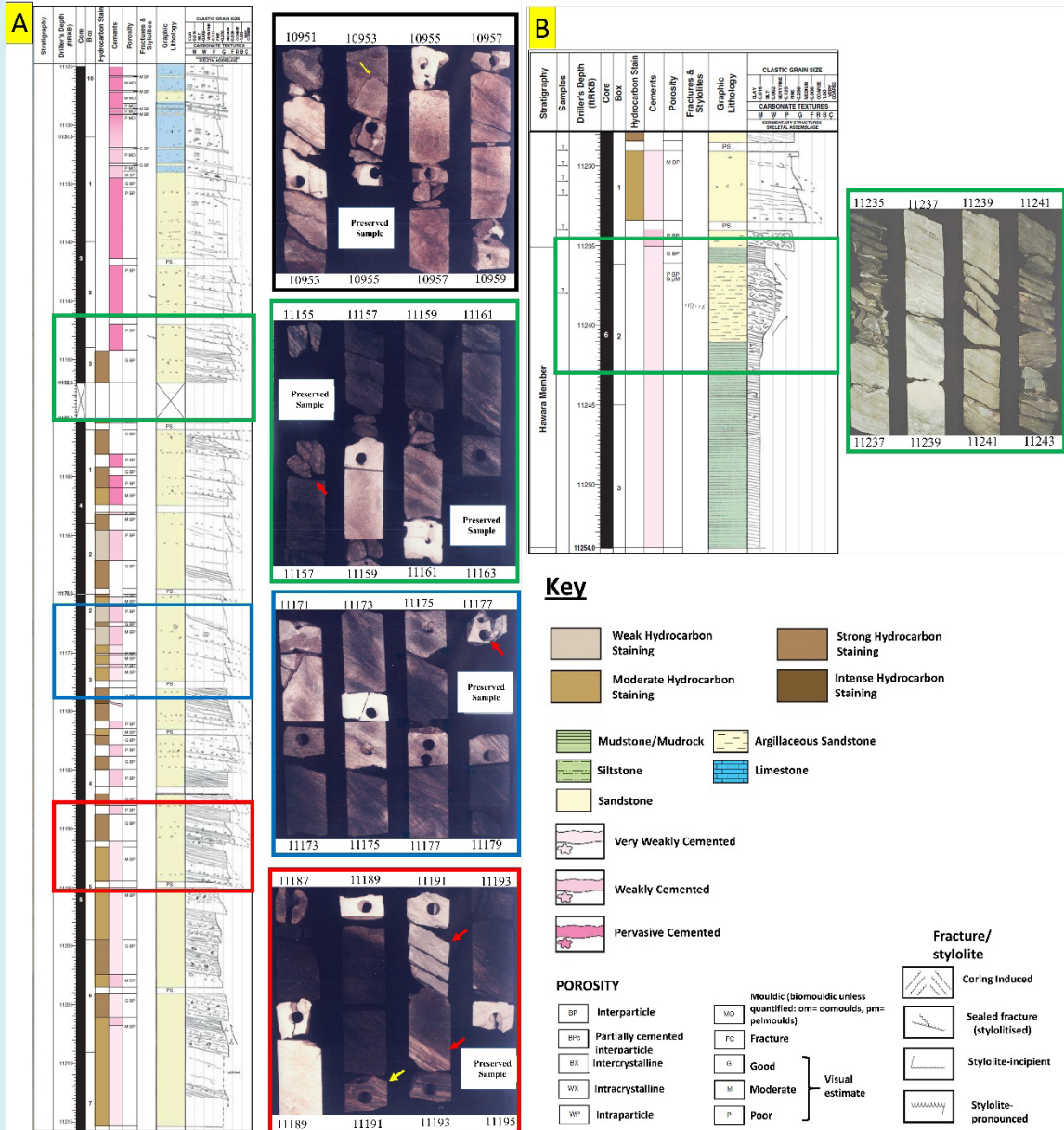


Figure 6: (A) core description log of OCT-J5 well presents the lithofacies composition, hydrocarbon staining, and cementation. (B) Core log and core a photograph showing the boundary between the deep marine lithofacies-A of Asl Member and the underlying pelagic shale of Hawara Member.

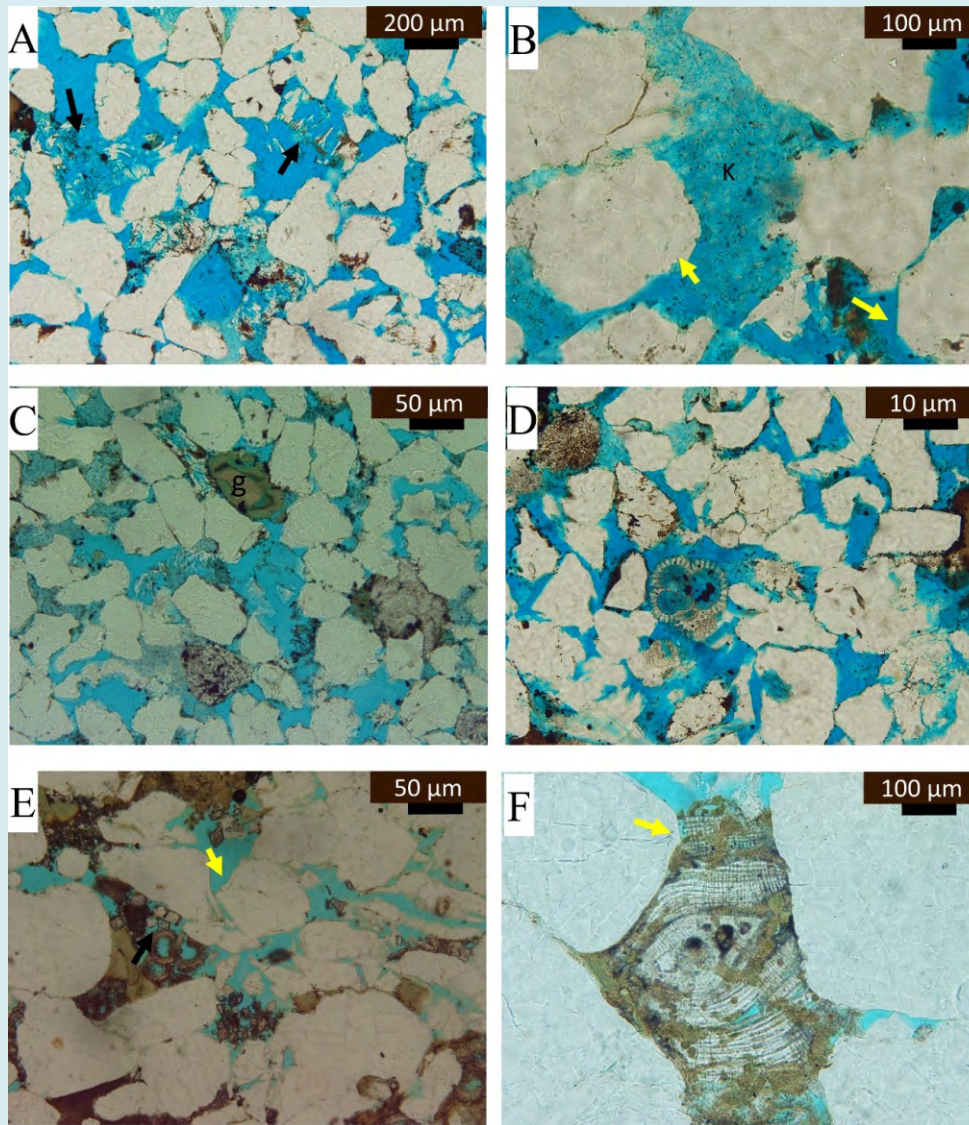


Figure 7: Sandstone lithofacies (A). (A) Arkosic quartz arenite with 25% porosity (blue dye epoxy), note the feldspars dissolution to form secondary porosity. Kaolinite clay infiltration can be observed within the pores. Fine clay film around the quartz grains (PPL). (B) Magnified micrographs present the kaolinite fabric (K) within the pore spaces which may act as a contributor to the microporosity. Faint silica overgrowth (yellow arrow) reduces the porosity (PPL). (C) Coarse grain well-sorted, porous quartz arenite with glauconitized fossiliferous pellets, spar calcite cementation (PPL)(D) Quartz arenite with primary intergranular porosity and secondary moldic porosity, metamorphic rock fragments in the upper left side. Clay cement partially filled the pores on the upper part. (E) Coarse-grained quartz arenite with reworked planktonic foraminifera and dolomite cementation (black arrow) (PPL). (F) Eocene large benthonic foraminifera reworked within the siliciclastic lithofacies (A) accommodation space. Also, silica overgrowth has been recognized (yellow arrow) (PPL).

Irregular erosional or sharp bases (Figure 8) characterize the sandstone beds. Sometimes, these beds show internal local fining upward with an overall general

trend of coarsening upward (Figure 7). Large-scale angular cross bedding, convolute bedding lamination and water escape structure are commonly observed (Figure 7);

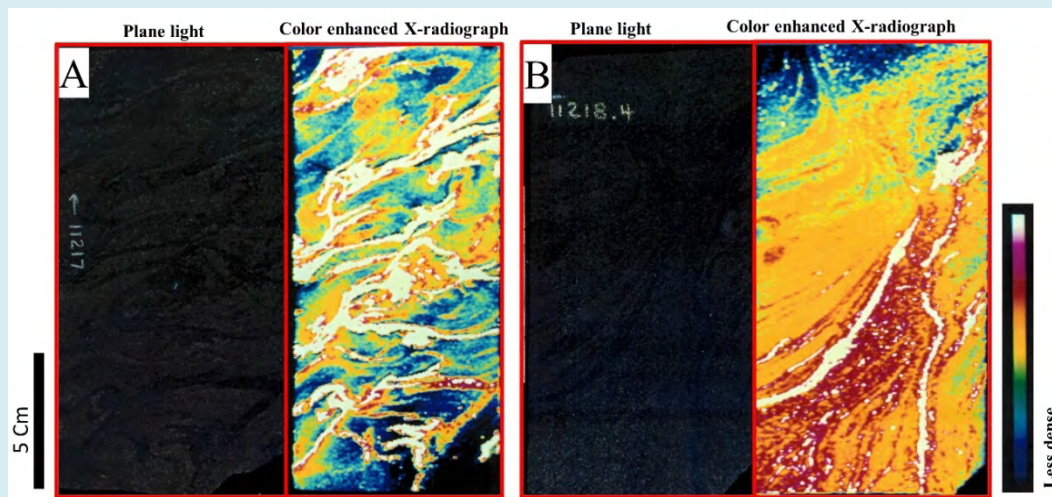


Figure 8: (A) Convolute lamination in sandstone at 11217 shown on the left is a plane light photograph of the sandstone core slab. Shown on the right is a color-enhanced X-radiograph image with a relative density scale imposed. The colors correspond to zones of high (white) and low (blue) X-ray absorption. Laminations are convolute and distorted due to rapid deposition and water escape that occurred 1.4 feet below. (B) Water escape structure in sandstone at 11218.4 shown on the left is a plane light photograph of the sandstone core slab. A large dewatering feature is apparent and becomes clearer in the color-enhanced X-radiograph image on the right. A relative density color scale is imposed showing high density (pink to white) where secondary cementation has occurred in the water escaped zone and lower density where overlying lamination has been punctured and turned upward.

The convolute disorder lamination and water escape structure observed in this sandstone reflect high energetic and rapid rate of sedimentation (Figure 8A). The enhanced colored x-radiography image shows white zones corresponding to high density (low porosity) and orange to blue zones of low-density (high porosity) (Figure 8). Secondary precipitation occurred in the water escaped zones, forming a white high-density image (Figure 8B). Image analyses show that within a distance of inches, rock properties change dramatically in some intervals, which are not readily apparent in plane light (Figure 8). This lithofacies show limestone interbeds ranging in thickness from one foot to a few inches. They consist of reworked skeletal carbonate containing sharp angular lithoclasts in a matrix of quartzose sandstone (Figure 8). In addition, two layers of one-foot thick consisting of bioturbated argillaceous calcareous sandstone are observed below 11191 ft depth (Figure 6).

Evans [13], Sallam, et al. [14] and Nabawy, et al. [11] reported that, the provenance of the Rudeis sandstone was primarily the exposed Nubia sandstones of the Western Sinai. The Asl sandstone (Upper Rudeis of the present study) in OCT-J5, OCT-F3B, and Tanka-3 wells is noticeably unlike the Nubia in composition and texture. It contains more feldspar (Figure 7), compared to the Nubia, which is typically over 95% quartz. Asl framework grains are much more angular suggesting a short transportation history and indicate a more granitic source area, with higher proportions

of fragmented Eocene benthic foraminifera (Figure 7F). These facts manifested that Asl sandstone may be derived from mixed provenance with less reworking in the sediment cycle. In addition, Asl sandstones do not seem similar to the unroofed Miocene sandstones described petrographically by Evans [13] from Wadi Gharandal which interpreted to be derived from an Eocene sediment source. Therefore, the Asl sandstone in the October Field I classified as subarkose, and derived from the nearby exposed basement in addition to Nubia and Eocene (Thebes/Radwany formations) sediments.

A thick conglomerate bed occurs at the well OCT-F3B (Figure 5A). It is located adjacent to the main bounding fault controlling the deposition and composed of sub-rounded quartz pebble (Figure 5A). Planar laminated bed tops locally display convolution (Figure 5C) and larger scale, chaotic soft-sediment deformation slumping features are observed in the overlying coarse-grained sandstone (Figure 5).

Shale Lithofacies: This lithofacies (2ft thick, Figure 4) represents the sole occurrence of shale within the Asl core and has a lithological resemblance to the underlying Hawara pelagic shale (Figure 6B; Figure 5B). Because of this resemblance and position between rapidly deposited sandstone, this shale is interpreted as a slump deposit. This interpretation favors high-energy conditions throughout the Asl deposition. An alternative explanation would be slow pelagic shale deposition between high-energy sand-bearing

turbidity flows.

Carbonate lithofacies: Carbonate lithofacies (C) range in color from off-white to light brown and can be classified as skeletal grainstone, packstone, and wackestone (Figure 9). The carbonate lithofacies are typically allochems and calcite cement supported with varying amounts of siliceous framework grains, i.e., quartz and feldspar. They are texturally and compositionally immature compared to the sandstones (Figure 9). The fabric is disorganized and variable. Constituents are medium to very coarse sand size, poor to moderately sorted, and angular to subrounded (Figure 9). Broken fossil fragments (5-75%) of benthic and planktonic foraminifera, bryozoans, echinoderms, algae, botryoidal grains and gastropods are recorded (Figure 9).

Silica framework grains account for 5 to 50% of the rock. Other minerals present in the carbonates include primary and allochthonous glauconite and secondary pyrite (Figure 9E). Scattered white to light brown pebble to cobble size carbonate fragments rich in planktonic foraminifera are interbedded within the limestone (Figures 4, 6, 7). The bioclast sizes range from fine-grained fragments to bivalves and bryozoan fronds that are several centimeters. The size variations reflect the bioclast source more than transport distance or mechanism [15,16]. Bioclasts are frequently completely cemented with non-ferroan calcite cement (Figure 9). The most common pore types are relatively isolated moldic (from the dissolution of bioclasts) and intraparticle (within the bioclasts) types (Figure 9A and D).

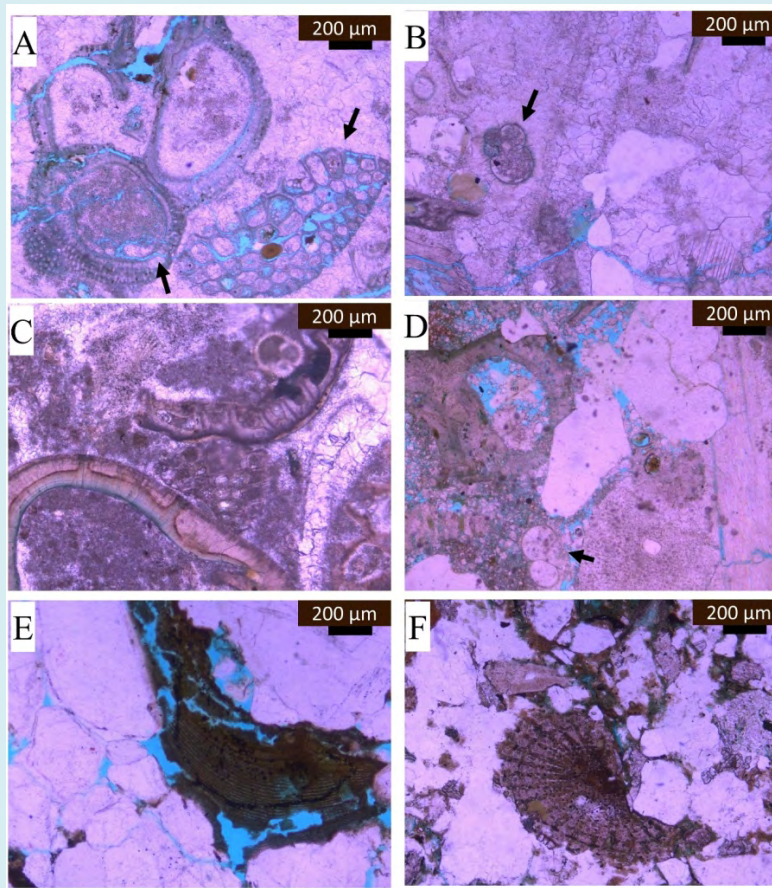


Figure 9: (A) Intraclasts grainstone. The intraclasts of botryoidal grains with intraparticle porosity (black arrows). Reworked green algae with dissolution porosity. Note the spar cement has filled the intergranular pores (PPL). (B) Foraminiferal wackestone with spar calcite filling the pores. Reworked blue-green algae of stromatolite and secondary dissolution porosity (PPL). (C) Pelecypod and shell fragment packstone, calcite has been micritized and the shell fragments filling with with spar calcite in parts (PPL). (D) Packstone of reworked algae with quartz grains. The algae have been dissolved to form secondary porosity enhancement (PPL). (E) Reworked algal fragments with preserved aragonite and shallow burial glauconitization with selective pyrite crystals filled the cast in parts. Intergranular primary porosity with secondary dissolved porosity exists (PPL). (F) Reworked foraminiferal shell with partially glauconitized (PPL).

Diagenesis of the Lithofacies

Petrographic examination shows evidence of both porosity enhancements by the dissolution of soluble components and porosity reduction by secondary mineralization and compaction. The diagenetic evolution of both sandstone (Lithofacies A) and carbonate (Lithofacies C) is shown in Figure 14.

Diagenesis in Sandstones (Lithofacies A)

Three main processes have acted to reduce primary intergranular porosity and reservoir quality over time. These are, in order from most to least influential:

- Formation of late-stage dolomite cement (Figure 10 A-D),
- Formation of quartz overgrowth cement (Figure 10 E-F),
- Formation of authigenic kaolinite clays (Figure 10D and 10A).

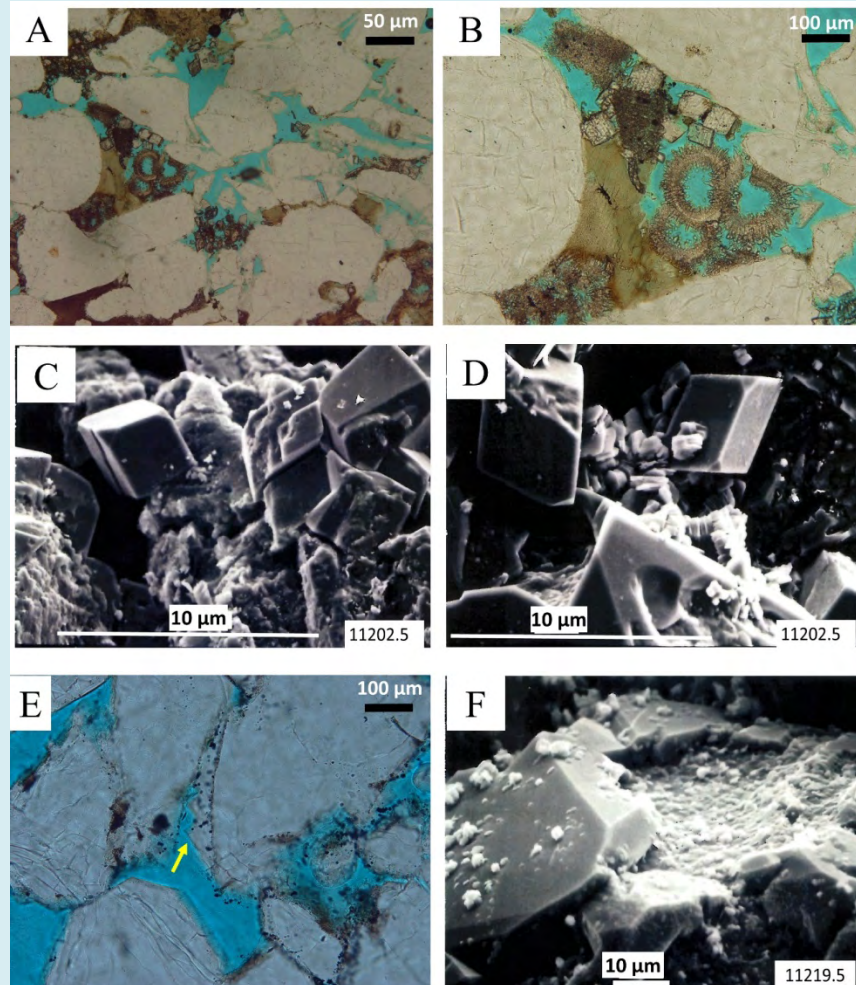


Figure 10: (A) and (B) Quartz arenite with primary intergranular and secondary intragranular porosity. Note the idiopathic form of the rhombic dolomite crystals at the late diagenetic stage. Glauconitization has partially occurred to reduce the porosity and reservoir quality (PPL). (C) SEM photomicrograph of the idiopathic dolomite rhombic crystals filling the primary pores and collapses the permeability at the late stage of diagenesis. (D) SEM photomicrograph of the idiopathic dolomite rhombic crystals with vermicular kaolinite precipitation that reduces the porosity and reservoir quality. (E) Intergranular porosity has been reduced by the syntaxial silica overgrowth (yellow arrow) with clay film around the quartz grains (PPL). (F) SEM of quartz overgrowth cementation in the sandstone.

The order of occurrence of these processes is based on textural relationships observed in thin sections and scanning

electron microscope (Figure 11).

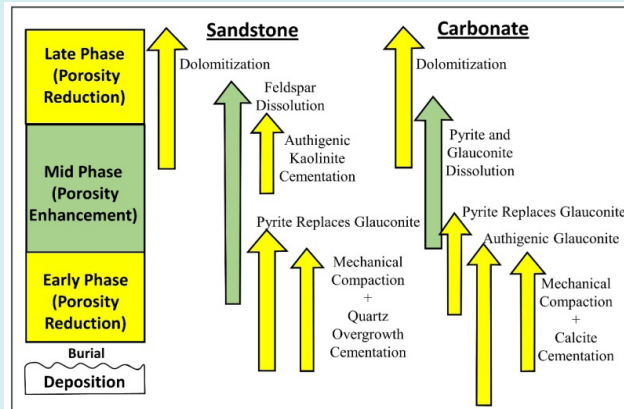


Figure 11: Diagenetic history of the Asl Member in October Field for lithofacies A and C with reservoir quality controllers.

Overall, the sandstones have retained very high primary intergranular porosity since deposition. This is concluded from the abundance of clean, open pore space and the lack of residual cement (Figure 7). Following deposition, silica-rich fluids, causing nucleation of syntaxial overgrowths onto

existing quartz grains, first affected the grains. Overgrowth textures are shown in OCT-J5 well only by the preservation of grain dust rims in thin sections (Figure 10E) and by three-dimensional preservation of terminated quartz crystal faces under SEM (Figure 10F).

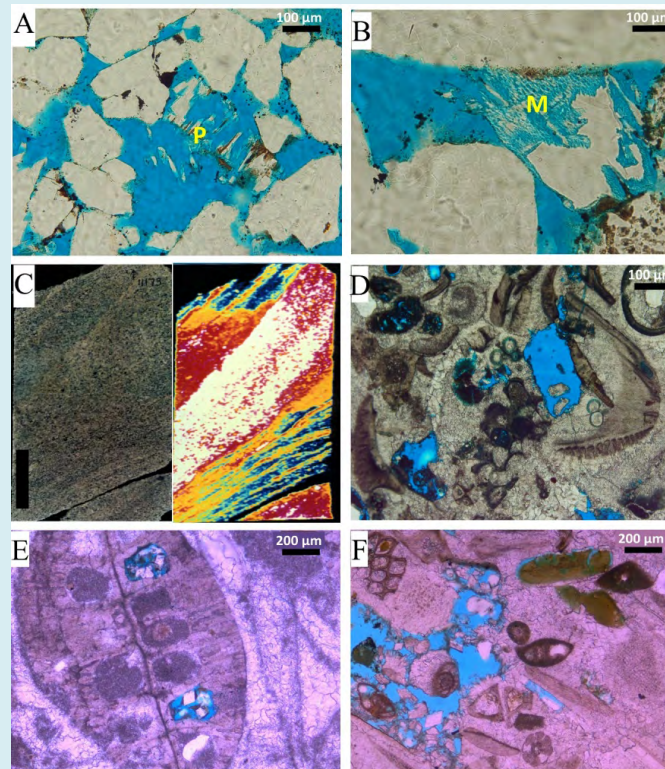


Figure 12: (A) Coarse-grained sandstone with enlarged porosity due to mineral degradation. Plagioclase (P) has been dissolved to form secondary porosity (PPL). (B) Dissolved labile microcline grain (M) and formation of secondary porosity (PPL). (C) X-radiograph image presents the high dense dolomite penetration in the sandstone. (D) Skeletal grainstone with botryoidal grains intraclasts. Intercrystalline porosity enhances the reservoir quality (PPL). (E) Reworked large foraminifera with quartz grains in the internal structure. Spar calcite act as late diagenetic cement with dolomite crystals filling the open cavities (PPL). (F) Grainstone with idiomorphic crystal rhombs manifest the late-stage of dolomitization. Intraclasts of Bryozoa grains on the upper left hand. Glauconitized green algae (green pellets) (PPL).

Preferred dissolution of plagioclase and potassium feldspar along twinning surfaces is observed (Figure 12A and B). In the more feldspar-rich rocks (5%-10%), porosity enhancement is estimated to be an additional 1% to 3%. Secondary pores created by feldspar dissolution are typically clean, showing no secondary pore-filling minerals (Figure 12A and B).

The formation of authigenic kaolinite, accounting for typically less than 5% of the rock, is observed (Figure 10D). It likely formed as a product of feldspar hydrolysis and played a minor role in further reducing primary porosity.

The most recent phase in the diagenetic history of the sandstones is a porosity-reducing process of dolomite cementation (Figure 11). The selected zones within the sandstone interval show evolving stages of dolomitization ranging from a few isolated dolomite rhombs occupying the pores (Figure 10B-D) to partially filled primary pores and significantly reducing permeability (Figure 10A and B). These dolomite rhombs are euhedral in form and grow

outward into open pores after nucleating on a preferred grain surface (Figure 10C-D). The white-pink zone in the sandstone image (Figure 12C) represents high density, tight dolomitized laminations.

Diagenesis in Carbonate (Lithofacies C)

The carbonate interval of the OCT-J5 well is a mix of fossil fragments, intraclasts, silicate grains, and rock fragments that have been significantly altered since deposition (Figure 12D-F). Processes acting to both reduce and enhance primary porosity in the carbonate are shown in Figure 14 in their relative order of occurrence. The order of most to least influential processes acting to reduce the reservoir quality:

- Formation of Late-stage dolomitization (Figure 12E and F),
- Formation of Early calcite cementation (Figure 12D),
- Formation of glauconitization in fossil fragments (Figure 13A and B),
- Pyritization of both autochthonous and allochthonous glauconite (Figure 13C to E).

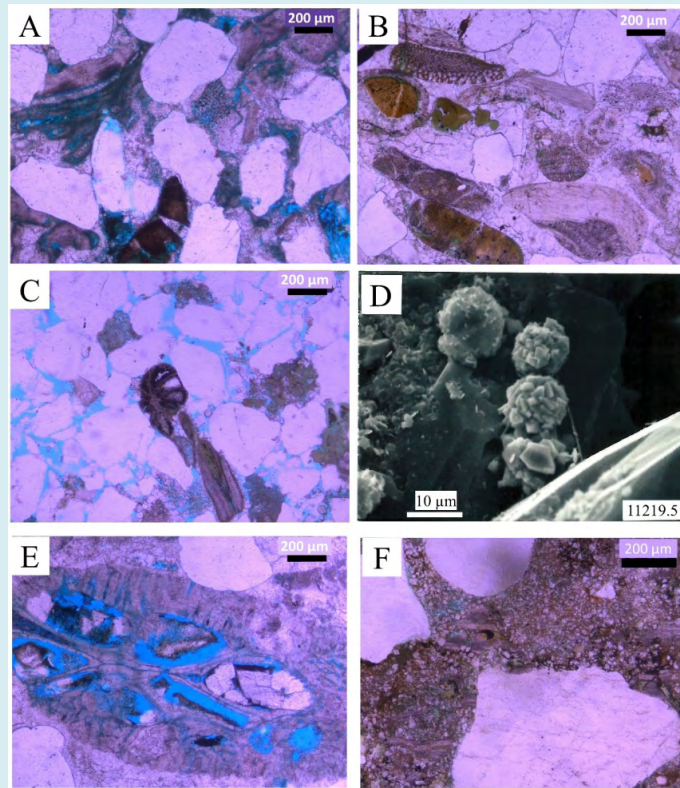


Figure 13: (A) Carbonate lithofacies with reworked sandstone and algae (PPL). (B) Skeletal and non-skeletal grainstone with reworked glauconitized red and green algae (PPL). (C) Sandstone with benthic foraminifera and shell fragments. Note the foraminifera have been partially pyritized calcite cementation fills the pores to reduce the reservoir quality in addition to the glauconite precipitation in parts (PPL). (D) SEM micrograph presents the pyrite precipitation around the quartz grains (PPL). (E) Reworked macroforaminifera with intraparticle secondary porosity and rhombic dolomite precipitation (PPL). (F) Late stage dolomitization fill the pore spaces and reduce the primary porosity (PPL).

The paragenetic sequence of these processes are in three stages. The first stage of diagenesis in the studied carbonate facies is the early porosity reduction by calcite cementation (Figure 11). On the other hand, fossil fragments bryozo, green algae, and foraminifera show body chambers completely or partially filled with glauconite, which reduce primary porosity (Figure 13B). The presence of glauconite, a potassium iron aluminosilicate, witness a marine depositional environment with close association with organic material [17,18,19]. This fact is consistent with the current interpretation of the Asl Member sediments. Afterthought pyritization the glauconite occurred and lead to further porosity reduction. The formation of pyrite crystals are seen either disseminated throughout a fossil fragment or growing as a coating around the glauconite pellets (Figure 13B-D).

The second stage of diagenesis of the carbonate is the porosity-enhancing dissolution of the glauconite and pyrite associated with the fossil material. Moldic pores (Figures 12 & 13) were formed through different stages of dissolution including early dissolution, where only a portion of the fossil has been dissolved, and late dissolution when practically the entire fossil has been dissolved.

The third phase of diagenesis in the carbonate is dolomitization. This process significantly reduces porosity and thus, reservoir quality (Figure 12E & F), whereas euhedral rhombs of dolomite occupy open pore spaces in varying stages of abundance. Dolomitization is a late-stage process because rhombs typically occupy moldic pores where the original organic matter and/or the secondary glauconite and pyrite have been dissolved away (Figure 13E). In more advanced stages of dolomitization, the original rock fabric has been obscured by interpenetrating dolomite rhombs in the OCT-J5 well, which in some cases reduces all primary pores and reservoir quality (Figure 13F).

Paragenetic Sequence

The sequence of diagenetic events in the Asl Member can be broadly subdivided into near-surface (Early-phase), shallow burial (Mid-phase), and deep burial (Late-Phase) phases (Figure 11). These phases are part of a continuum, and diagenetic events occurring within them will necessarily overlap to some degree. The events listed below are the dominant ones for each phase:

Near-surface diagenesis (Early-Phase): The pore-filling and intraparticle fibrous cement were originally precipitated in the marine realm as aragonite. This aragonite cement has been converted with time to non-ferroan calcite. The calcite cement occurs within the chambers of the bioclasts but occluded only the small pores (Figures 10-13).

Mechanical compaction occurred after deposition by rapid burial as a result of high rate of sedimentation (Figure 11). These conditions were favored by the accommodation space created at the hanging wall of the rotated tilted fault blocks at the propagation stage of rifting.

The syntaxial quartz overgrowth observed in the sandstone lithofacies of the OCT-J5 well. It was generated earlier in the paragenetic sequence in sizes ranging from 5-15 μm of lithofacies (A) [20]. The source of silica overgrowth was suggested as the effect of pressure solution that was supposed to be initiated during the Clysmic fault propagation phase as interpreted from burial history modeling. In addition, the quartz overgrowth has not been recognized in the Tanka-3 well, which is more basinal with thermal heating below 100 °C [20].

Shallow burial diagenesis: The dissolution of aragonitic bioclasts has contributed extensively and originally to enhancing the reservoir quality (Figures 12 & 13). Such dissolution occurs by pore fluids that are under-saturated with calcite and is commonly later expelled due to overburden pressure. Subsequent pore-filling cementation destroyed reservoir quality.

Deep burial diagenesis: The pore filling by dolomite and calcite cement is an important diagenetic event because it fills most of the inter and intraparticle secondary macropores (Figures 12 & 13) in both carbonate and siliciclastic dominated lithofacies. Mechanical compaction is remarkable through the sedimentary burial history and has reduced primary intergranular pores, especially in siliciclastic lithofacies (A) (Figure 10).

The cores show a range of hydrocarbon stains (Figure 6), from pervasive and intense, to minor or none. As the majority of cementation occurred late in the diagenetic history and hence absence of hydrocarbons in the cemented lithologies, the main charge is considered to have post-dated the deep burial of the reservoir.

Impact of Diagenesis on Reservoir Quality

The reservoirs occur in the ~ 200 ft-thick-lower part of the Asl Member and consist of fine- to coarse-grained turbidite sandstones. They are locally derived heterogeneous with variable porosity and permeability ranging from 17-27% and 30-3000 mD, respectively. The carbonates are also heterogeneous, ranging from skeletal grainstones to packstones, with porosity and permeability of 3-17% and 0.01-90 mD, respectively. Based on core and thin section investigation, three main processes have acted to reduce primary intergranular porosity and reservoir quality over time in the sandstone lithofacies (A). These are, in order from

most to least influential Formation of late-stage dolomite cement, quartz overgrowth cement, and authigenic kaolinite clays, while the dissolution of feldspars, contributes to enhancing the pore system. For the carbonate lithofacies (C), the formation of late-stage dolomite, early calcite cement, glauconite in fossil fragments, and pyrite crystals after both autochthonous and allochthonous glauconite. On the other side, porosity enhancement in carbonates occurred through the dissolution of detrital and the replacement of glauconite within the fossil fragments.

The reservoir quality varies between the lithofacies in the studied wells. Sandstone lithofacies (A) is in general more porous and permeable than carbonate packstones and grainstones lithofacies (C). Measured porosity and permeability of lithofacies (A) are notably high, ranging from 15 to 28% and 10 to 4000mD, respectively (Figure 14A). Discriminating the OCT-J5 well based on the porosity permeability variables, the lithofacies (A) found in higher porosity-permeability values than lithofacies (C) (Figure 14B). The Pore filling, non-ferroan calcite, and dolomite cement, in addition to silica overgrowth, are the major factors control the reservoir quality degradation in the cored intervals (Figures 10-13). The above-mentioned cement occurs in bioclast body cavities, interparticle pores, moldic pores, and fractures. It is the dominant cement phase in carbonate, in mixed carbonate-siliciclastic and siliciclastic lithofacies. Thinner sandstone units that are surrounded by carbonate-rich lithologies may be completely cemented

by calcite (Figure 6). In addition to calcite cement, bioclast fragments, ductile grains (e.g., glauconite) deform with the matrix and occlude interparticle pores in sandstones (Figures 7F & 9). This type of material tends to occur in layers and can have a detrimental effect on vertical permeability, especially where compaction is extensive. Fine-grained sandstones are often more adversely affected by abundant matrix material and compaction than coarse sandstones and have a correspondingly increased reduction in porosity and permeability [20].

To sum up, the ability to predict the presence and distribution of reservoir properties is vital to the successful exploitation of a reservoir. In the Asl Member, porosity and permeability values vary greatly in both carbonate-dominated and siliciclastic-dominated lithofacies in vertical and lateral dimensions. Although packstones and grainstones may have good porosity values (10-20%), the moldic and intraparticle pores tend to be poorly connected. Hence, permeability values are rarely greater than 10mD (Figure 14). The distribution of these lithofacies is complex and difficult to predict, but they seem to be most common on shallower portions of rotated fault blocks. The thickness of carbonate-dominated units thins away from the fault blocks and the detrimental effects of calcite cementation should decrease. Other factors such as sandstone thickness must be taken into consideration when evaluating the influence of cementation.

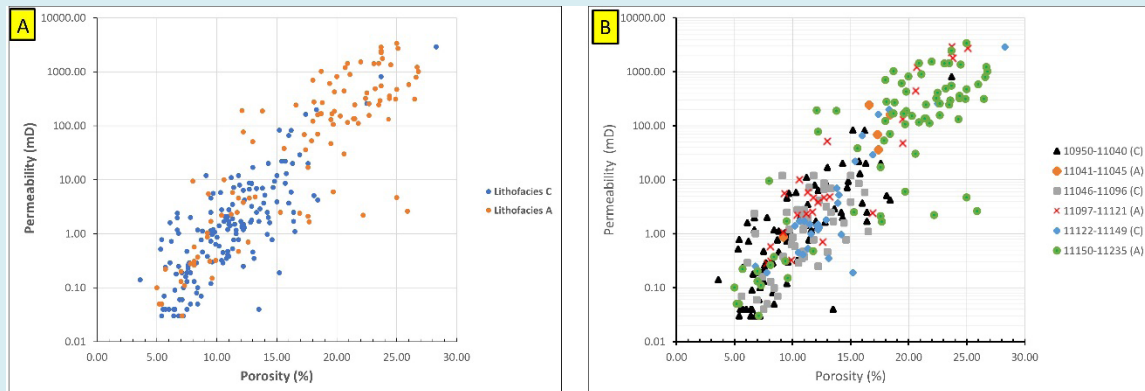


Figure 14: (A) Measured porosity and permeability cross plots from routine core analysis of OCT-J5 core present the higher reservoir quality in lithofacies-A regarding lithofacies-C. (B) porosity and permeability presentation with depth. Note the high porosity and permeability values found at the highest depth of the Asl Sandstone Member.

Fine-grained, distal sandstones may have good reservoir properties, but the coarse-grained sandstones contribute to the bulk products from the Asl reservoir. The thicker the sandstone interval, the greater the chance that a significant proportion of the interval will be only lightly cemented and that connected interparticle porosity has been preserved. However, the majority of even 50ft intervals may be moderate

to extensively cement (e.g., Tanka-3, 9963-10013ft, Figures 5 & 6), and thinner intervals are usually adversely affected by calcite cement. Thick, proximal to mid-fan sandstones located close to rift faults, and to their intersections with cross faults will provide the best combination of depositional and diagenetic characteristics for preserving good reservoir quality.

Conclusions

The petrographic analysis, thermal burial history, core description and surface section integration of the Asl Member unlocked the sedimentological and diagenetic characteristics of the propagation stage of rift mixed sediments. The repeatedly coarse-grained lithofacies (A), fine-grained lithofacies (B) and lithofacies (C) reflect variations in gross depositional processes, environments and architecture. The carbonate lithofacies (C) initially deposited on upraised rotated fault blocks were mixed and interbedded with siliciclastic lithofacies that were initially derived from exposed older source areas (Eocene sediments). The coarse-grained sandstones occur in proximal locations on the submarine fan, whereas finer-grained sandstones are increasingly interbedded in more mid to distal settings. The Pre-Miocene (Pre-rift) materials of Wadi Feiran and Wadi Baba accommodate the clastic and carbonate lithofacies via canyon or between the relay ramps of the propagated extensional faults. The dolomite, quartz cement and authigenic kaolinite clays are the main processes reduce the reservoir quality. While, the dissolution of feldspars enhancing the pore system in the sandstone lithofacies (A). In contrast, late stage dolomite, early calcite cements, glauconitization and pyritization reduced the quality in carbonate lithofacies (C). Degradation and destruction of the reservoir quality are primarily due to an abundance of non-Ferron calcite pore filling, in the mixed carbonate-siliciclastic and siliciclastic-dominated lithofacies, especially where sandstone beds are thin and encased by carbonate units. The best reservoir quality occurs in sandstones in the lower 100-150 ft of the Asl Member, above the underlying shales of the Hawara Member.

References

1. Lelek JJ, Shepherd DB, Stone DM, Abdine AS (1992) October Field - the latest giant under development in Egypt's Gulf of Suez. In: Halbouty MT (Ed.), Giant Oil and Gas Fields of the Decade 1978- 1988. AAPG Memoir 54: 231-249.
2. Kassem AA, Osman OA, Nabawy BS, Baghdady AR, Shehata AA (2022) Microfacies analysis and reservoir discrimination of channelized carbonate platform systems: An example from the Turonian Wata Formation, Gulf of Suez, Egypt. J Pet Sci Eng 212: 110272.
3. Kassem AA, Sharaf LM, Baghdady AR, El-Naby AA (2020) Cenomanian/Turonian oceanic anoxic event 2 in October oil field, central Gulf of Suez, Egypt. J Afr Earth Sci 165: 103817.
4. Robson DA (1971) The structure of the Gulf of Suez (Clysmic) rift, with special reference to the eastern side. J Geol Soc 127(3): 247-271.
5. Alsharhan AS (2003) Petroleum geology and potential hydrocarbon plays in the Gulf of Suez rift basin. AAPG Bull 87(1): 143-180.
6. Radwan AE, Kassem AA, Kassem A (2020) Radwany Formation: A new formation name for the Early-Middle Eocene carbonate sediments of the offshore October oil field, Gulf of Suez: Contribution to the Eocene sediments in Egypt. Mar Pet Geol 116: 104304.
7. Radwan AE, Trippetta F, Kassem AA, Kania M (2021) Multi-scale characterization of unconventional tight carbonate reservoir: Insights from October oil field, Gulf of Suez rift basin, Egypt. J Pet Sci Eng 197: 107968.
8. Bosworth W, Crevello P, Winn, RD, Steinmetz J (1998) Structure, sedimentation, and basin dynamics during rifting of the Gulf of Suez and north-western Red Sea. In: Purser BH, et al. (Eds.), Sedimentation and tectonics in rift basins red sea: Gulf of Aden. Springer, Dordrecht, pp: 77-96.
9. Wescott WA, Krebs WN, Dolson JC, Karamat SA, Nummedal D (1996) Rift basin sequence stratigraphy: some examples from the Gulf of Suez. GeoArabia 1(2): 343-358.
10. Lashin A, Al-Arifi N, Ashour NA (2011) Evaluation of the ASL and Hawara members using seismic-and log-derived properties, October Oil Field, Gulf of Suez, Egypt. Arab J Geosci 4(3-4): 365-383.
11. Nabawy BS, Mansour AS, Rashed MA, Afify WS (2020) Implementation of sedimentary facies and diagenesis on the reservoir quality of the Aquitanian-Burdigalian Rudeis Formation in the Gulf of Suez, Egypt: A comparative surface and subsurface study. Geol J 55(6): 4543-4563.
12. Stone DM (1992) Reservoir description and depositional environment of the Asl Member, North October Field, Gulf of Suez, Egypt. EGPC Exploration and Production Conference, Cairo, 1: 194-228.
13. Evans AL (1990) Miocene sandstone provenance relations in the Gulf of Suez: insights into synrift unroofing and uplift history. AAPG Bull 74(9): 1386-1400.
14. Sallam ES, Afife MM, Fares M, van Loon AJ, Ruban DA (2019) Sedimentary facies and diagenesis of the Lower Miocene Rudeis Formation (southwestern offshore margin of the Gulf of Suez, Egypt) and implications for its reservoir quality. Mar Geol 413: 48-70.

15. Bornhold BD, Pilkey OH (1971) Bioclastic turbidite sedimentation in Columbus basin, Bahamas. *GSA Bull* 82(5): 1341-1354.
16. Zhang J, Liu G, Cao Z, Tao S, Felix M, et al. (2019) Characteristics and formation mechanism of multi-source mixed sedimentary rocks in a saline lake, a case study of the Permian Lucaogou Formation in the Jimusaer Sag, northwest China. *Mar Pet Geol* 102: 704-724.
17. Berner RA (1981) A new geochemical classification of sedimentary environments. *J Sediment Res* 51(2): 359-365.
18. Udgata D (2007) Glauconite as an indicator of sequence stratigraphic packages in a lower Paleocene passive-margin shelf succession, Central Alabama. Dissertation, Auburn University, USA.
19. Rudmin M, Banerjee S, Mazurov A (2017) Compositional variation of glauconites in Upper Cretaceous-Paleogene sedimentary iron-ore deposits in South-eastern Western Siberia. *Sediment Geol* 355: 20-30.
20. Lawan AY, Worden RH, Utley JE, Crowley SF (2021) Sedimentological and diagenetic controls on the reservoir quality of marginal marine sandstones buried to moderate depths and temperatures: Brent Province, UK North Sea. *Mar Pet Geol* 128: 104993.

